

Chapter 4

An Enriched Formulation for Plate Fracture

In this chapter, the use of discontinuous enrichment to model the fracture of Mindlin-Reissner plates is examined. The Mindlin-Reissner plate theory is attractive from a finite element modeling standpoint for several reasons. Imposing a few kinematic assumptions on the governing equations, the Mindlin-Reissner model provides a two-dimensional approximation of thin three-dimensional plates subjected to bending. In contrast to the Kirchhoff plate formulation, the Mindlin theory allows for transverse shear strains which relaxes the continuity requirements on the approximating space. In fracture analysis, the Mindlin theory also predicts the expected angular distribution of the stress fields near the crack tip. At first glance, the enrichment of a plate formulation may seem to be a straightforward extension of the two-dimensional derivation presented in the previous chapter. However, several difficulties are associated with the finite element modeling of mixed-mode fracture in Mindlin-Reissner plates.

Much of the theoretical groundwork for plate fracture in the Mindlin-Reissner formulation was developed in Knowles and Wang (1960), who derived the analytical solution for the moment and shear fields near the crack tip. The definition of moment and shear force intensity factors can be found in Sih (1977), in addition to analytical solutions for some simple geometries. Unfortunately, many of these solutions were shown to be incorrect for thin plates (Joseph and Erdogan, 1991). More recent analytical and numerical results are limited to simple geometries, and quite often are only available for pure Mode I loadings. One reason for the latter is the apparent lack of a suitable method to extract the mixed-mode intensity factors. While some work has been performed in this area (Sosa and Herrmann, 1989), (Sosa and Eischen, 1986), the derived contour integrals are not well suited to finite element calculations, and in some cases only accomplish part of the task.

An additional complication is the phenomenon known as shear locking. As the plate becomes very thin, both the solution and its approximation must satisfy the constraint that the transverse shear strains vanish in the domain. When there are not enough functions in the finite element subspace which satisfy this constraint, a poor approximation results for the plate displacements. Fortunately, plate elements have been developed which do not exhibit shear locking. See Pitkäranta and Suri (1996) for an excellent review of several plate elements and the pertinent issues. Concerning the modeling of fracture, the free surface of the crack faces presents additional challenges, and some elements perform much better than others (Pitkäranta and Suri, 1998). Numerical studies of plate fracture often use less robust formulations, and examine only relatively thick plates.

In this chapter, we examine the discontinuous enrichment of a plate element which does not exhibit shear locking, with the goal of modeling mixed-mode plate fracture.

In the following section, the governing equations and variational formulation are reviewed for Mindlin-Reissner plates. A standard discrete approximation which avoids shear locking is also discussed. In Section 4.3, a domain form of an interaction integral for plates is developed to extract the mixed-mode intensity factors. The enriched discretization is given in Section 4.4, and approximate solutions to benchmark problems in Section 4.5 illustrate the accuracy and robustness of the proposed formulation. Closing remarks are given in the final section.

4.1 Problem Formulation

There are several different ways to introduce the Mindlin theory. In this section, the governing equations are developed from a degeneration of the three-dimensional elasticity problem using the principle of virtual work with the appropriate kinematic assumptions.

4.1.1 Governing Equations

Consider the domain $\Omega \subset \mathcal{R}^2$ with boundary Γ which represents the midplane of a plate with thickness t occupying the region $\Omega \times (-t/2, t/2)$. The conventions adopted in this chapter are shown in Fig. 4.1. The main assumptions of the Mindlin theory state that the in plane displacements, u_1 and u_2 vary linearly through the thickness with the section rotations ψ_1 and ψ_2 . In addition, the normal stress σ_{33} is assumed to vanish in the domain. We make the additional assumptions that the surfaces of the plate ($x_3 = h/2, -h/2$) and any crack faces are traction-free.

In the $(\mathbf{e}_1, \mathbf{e}_2, \mathbf{e}_3)$ basis, where \mathbf{e}_3 is the unit normal vector to the plate, the

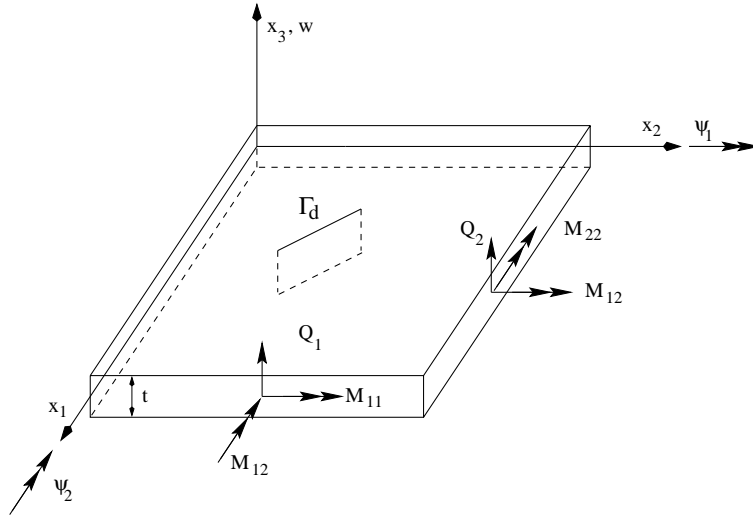


Figure 4.1: Notations and sign conventions for a plate with a through crack.

displacement components at a point (x_1, x_2, x_3) are given by

$$\mathbf{u}(\mathbf{x}) = \begin{cases} u_1 = x_3 \psi_1(x_1, x_2) \\ u_2 = x_3 \psi_2(x_1, x_2) \\ u_3 = w(x_1, x_2) \end{cases} \quad (4.1)$$

where w is the transverse displacement and ψ_1 and ψ_2 are section rotations about the x_2 and x_1 axes, respectively. The above can be expressed in a more compact form as

$$\mathbf{u}(\mathbf{x}) = w \mathbf{e}_3 + x_3 \boldsymbol{\psi} \quad (4.2)$$

where $\boldsymbol{\psi} = \psi_1 \mathbf{e}_1 + \psi_2 \mathbf{e}_2$.

The strain is given by

$$\frac{1}{2}(\nabla \mathbf{u} + (\nabla \mathbf{u})^t) = x_3 \boldsymbol{\epsilon}_b(\boldsymbol{\psi}) + \frac{1}{2}(\boldsymbol{\epsilon}_s(w, \boldsymbol{\psi}) \otimes \mathbf{e}_3 + \mathbf{e}_3 \otimes \boldsymbol{\epsilon}_s(w, \boldsymbol{\psi})) \quad (4.3)$$

with the bending contribution

$$\boldsymbol{\epsilon}_b(\boldsymbol{\psi}) = \frac{1}{2} (\nabla \boldsymbol{\psi} + (\nabla \boldsymbol{\psi})^t) \quad (4.4)$$

and a shear contribution

$$\boldsymbol{\epsilon}_s(w, \boldsymbol{\psi}) = \nabla w + \boldsymbol{\psi} \quad (4.5)$$

We note that the \mathbf{e}_3 related components are zero for both $\boldsymbol{\epsilon}_b$ and $\boldsymbol{\epsilon}_s$.

The virtual internal work is defined by

$$\delta W^{int} = \int_{\Omega} \boldsymbol{\sigma} : \nabla(\delta \mathbf{u}) \, d\Omega \quad (4.6)$$

where $\boldsymbol{\sigma}$ is the symmetric stress tensor, and $\delta \mathbf{u}$ is an arbitrary virtual displacement from the current position. After a few manipulations, we obtain the relation

$$\boldsymbol{\sigma} : \nabla(\delta \mathbf{u}) = x_3 \boldsymbol{\sigma}^\pi : \boldsymbol{\epsilon}_b(\delta \boldsymbol{\psi}) + \boldsymbol{\sigma}^s \cdot \boldsymbol{\epsilon}_s(\delta w, \delta \boldsymbol{\psi}) \quad (4.7)$$

where the π superscript indicates a reduction of the operator to the in plane ($\mathbf{e}_1, \mathbf{e}_2$) components and $\boldsymbol{\sigma}^s$ is the shear stress vector $\boldsymbol{\sigma}^s = \boldsymbol{\sigma} \cdot \mathbf{e}_3$.

Making the substitution (4.7) into (4.6) and integrating through the thickness gives the work expression

$$\delta W^{int} = \int_{\Omega} (\mathbf{M} : \boldsymbol{\epsilon}_b(\boldsymbol{\psi}) + \mathbf{Q} \cdot \boldsymbol{\epsilon}_s(w, \boldsymbol{\psi})) \, d\Omega \quad (4.8)$$

where the moment \mathbf{M} and shear \mathbf{Q} are defined by

$$\mathbf{M} = \int_{-t/2}^{t/2} x_3 \boldsymbol{\sigma}^\pi dx_3 \quad \mathbf{Q} = \int_{-t/2}^{t/2} \boldsymbol{\sigma}^s dx_3 \quad (4.9)$$

The virtual external work is composed of the action of the bending and twisting moments gathered in a couple vector \mathbf{C} , and of the shear traction \mathbf{T} . As previously stated, we assume there is no external pressure acting on the plate. The virtual external work is then

$$\delta W^{ext} = \int_{\Gamma} \mathbf{C} \cdot \delta \boldsymbol{\psi} d\Gamma + \int_{\Gamma} \mathbf{T} \delta w d\Gamma \quad (4.10)$$

Equating the internal and external virtual work, and applying the divergence theorem yields the equilibrium equations in Ω

$$\nabla \cdot \mathbf{M} - \mathbf{Q} = 0 \quad (4.11a)$$

$$\nabla \cdot \mathbf{Q} = 0 \quad (4.11b)$$

and the traction boundary conditions on Γ

$$\mathbf{C} = \mathbf{M} \cdot \mathbf{n} \quad (4.12a)$$

$$\mathbf{T} = \mathbf{Q} \cdot \mathbf{n} \quad (4.12b)$$

where \mathbf{n} is the unit outward normal to the boundary.

The constitutive relationships are obtained by energetic equivalence between the plate and the three-dimensional model. Assuming the plate is made of an isotropic homogeneous elastic material of Young's modulus E and of Poisson's ratio ν , the

constitutive relations are given by

$$\begin{bmatrix} M_{11} \\ M_{22} \\ M_{12} \end{bmatrix} = \frac{Et^3}{12(1-\nu^2)} \begin{bmatrix} 1 & \nu & 0 \\ \nu & 1 & 0 \\ 0 & 0 & 1-\nu \end{bmatrix} \begin{bmatrix} \epsilon_{b11} \\ \epsilon_{b22} \\ \epsilon_{b12} \end{bmatrix} \quad (4.13)$$

and

$$\begin{bmatrix} Q_1 \\ Q_2 \end{bmatrix} = \frac{Ekt}{2(1+\nu)} \begin{bmatrix} \epsilon_{s1} \\ \epsilon_{s2} \end{bmatrix} \quad (4.14)$$

where $k = 5/6$ is a correction factor which accounts for the parabolic variation of the transverse shear stresses through the thickness of the plate.

The above equations can be rewritten in a more compact form using the fourth order bending stiffness tensor \mathbf{D}_b and the second order shear stiffness tensor \mathbf{D}_s :

$$\mathbf{M} = \mathbf{D}_b \boldsymbol{\epsilon}_b \quad \mathbf{Q} = \mathbf{D}_s \boldsymbol{\epsilon}_s \quad (4.15)$$

4.1.2 Variational Formulation

Let the boundary Γ be divided into a part Γ_u on which kinematic boundary conditions $(w_g, \boldsymbol{\psi}_g)$ are imposed and a part Γ_t on which loads are applied with the restrictions

$$\Gamma = \Gamma_u \cup \Gamma_t \quad \Gamma_u \cap \Gamma_t = \emptyset. \quad (4.16)$$

The kinematics constraints are given by a prescribed transverse displacement w and prescribed rotations $\boldsymbol{\psi}$ while the loads come from the prescribed couples \mathbf{C} and prescribed shear tractions \mathbf{T} . As in Chapter 3, we also designate Γ_d as an internal

boundary across which the displacement field is allowed to be discontinuous.

Let \mathcal{U} be the space of kinematically admissible transverse displacements and rotations:

$$\mathcal{U} = \{(w, \boldsymbol{\psi}) \in \mathcal{V} : w = w_g, \boldsymbol{\psi} = \boldsymbol{\psi}_g \quad \text{on } \Gamma_u\} \quad (4.17)$$

where \mathcal{V} is a space of sufficiently smooth functions on Ω . As in Chapter 3, we leave the details on the regularity of the space to Babuška and Rosenzweig (1972) and Grisvard (1985). We note that the space \mathcal{V} allows for discontinuous functions across Γ_d .

The space of test functions is defined similarly as:

$$\mathcal{U}_0 = \{(w, \boldsymbol{\psi}) \in \mathcal{V} : w = 0, \boldsymbol{\psi} = 0 \quad \text{on } \Gamma_u\} \quad (4.18)$$

The weak form is to find $(w, \boldsymbol{\psi}) \in \mathcal{U}$ such that

$$\begin{aligned} \int_{\Omega} (\mathbf{D}_b \boldsymbol{\epsilon}_b(\boldsymbol{\psi})) : \boldsymbol{\epsilon}_b(\delta \boldsymbol{\psi}) \, d\Omega + \int_{\Omega} (\mathbf{D}_s \boldsymbol{\epsilon}_s(w, \boldsymbol{\psi})) \cdot \boldsymbol{\epsilon}_s(\delta w, \delta \boldsymbol{\psi}) \, d\Omega = \\ \int_{\Gamma} \mathbf{C} \cdot \delta \boldsymbol{\psi} \, d\Gamma + \int_{\Gamma} \mathbf{T} \delta w \, d\Gamma \quad \forall (\delta w, \delta \boldsymbol{\psi}) \in \mathcal{U}_0 \end{aligned} \quad (4.19)$$

It can be shown that the above is equivalent to the equilibrium equations (4.11) and traction boundary conditions (4.12). When the space \mathcal{V} is discontinuous along Γ_c , the traction-free conditions on the crack faces are also satisfied.

4.2 Discretization with the MITC4 plate element

When discretizing the plate equations (4.11), some care must be taken for thin plates. As the plate becomes very thin, the following relationship must be satisfied to keep the strain energy in the plate bounded:

$$\nabla w + \boldsymbol{\psi} = 0 \quad (4.20)$$

In other words, the shear strain $\boldsymbol{\epsilon}_s$ must vanish in the domain as $t \rightarrow 0$. This condition is known as the Kirchhoff constraint, and it applies to both the solution $(w, \boldsymbol{\psi})$ and its approximation $(w^h, \boldsymbol{\psi}^h)$. When there are not enough functions in \mathcal{V}^h which satisfy (4.20), a degradation in the accuracy and initial rates of convergence is observed for the plate displacements $(w^h, \boldsymbol{\psi}^h)$. This phenomenon is often referred to as shear locking.

Several different element formulations have been developed to address the shear locking issue. A consideration when dealing with plate fracture is the element performance near the free surface of the crack faces, and in this regard the MITC class of elements (Bathe, Bucalem, and Brezzi, 1990) offer superior performance over other available formulations (see the analysis of Pitkäranta and Suri (1996)). In the present investigation, we consider only the MITC4 element, whose approximation is based on the 4-node isoparametric quadrilateral. In the following, we review only the standard approximation. The modifications made for the enrichment of the element are presented in Section 4.4.

Let us assume that we have a triangulation of the domain Ω and that each element is a quadrilateral. Each element E is the image of a reference quadrilateral \hat{E} through an affine invertible mapping: $\boldsymbol{x} = \boldsymbol{x}(\boldsymbol{\xi})$ $\boldsymbol{\xi} \in [-1, 1] \times [-1, 1]$. On each element

the transverse displacement field is expressed in terms of the four nodal coefficients $w_i, i = 1, \dots, 4$ through the classical bilinear shape functions ϕ_i :

$$w^h(\mathbf{x}) = \sum_{i=1}^4 \phi_i(\boldsymbol{\xi}(\mathbf{x})) w_i, \quad \mathbf{x} \in E, \quad \boldsymbol{\xi} \in \hat{E} \quad (4.21)$$

The rotation field in the bending term (the first term in (4.19)) also uses the classical bilinear shape functions; the degrees of freedom being the \mathbf{e}_1 and \mathbf{e}_2 components of the vector $\boldsymbol{\psi}$ at each of the four nodes of the element:

$$\boldsymbol{\psi}(\mathbf{x}) = \sum_{i=1}^4 (\phi_i(\boldsymbol{\xi}(\mathbf{x})) \psi_{i1} + \phi_i(\boldsymbol{\xi}(\mathbf{x})) \psi_{i2}), \quad \mathbf{x} \in E, \quad \boldsymbol{\xi} \in \hat{E} \quad (4.22)$$

In order to avoid shear locking, a modification is made to the shape functions for the approximation of the rotation vector in the shear term (second term in (4.19)). We denote these special shape functions as $\tilde{\phi}_{i1}$ or $\tilde{\phi}_{i2}, i = 1, \dots, 4$ as they are related to ψ_{i1} or ψ_{i2} , respectively.

$$\boldsymbol{\psi}(\mathbf{x}) = \sum_{I=1}^4 (\tilde{\phi}_{i1}(\mathbf{x}) \psi_{i1} + \tilde{\phi}_{i2}(\mathbf{x}) \psi_{i2}), \quad \mathbf{x} \in E \quad (4.23)$$

Let $\{w_i\}$ be the set of all transverse displacement degrees of freedom and $\{\boldsymbol{\psi}_i\}$ the set of all rotational degrees of freedom, including both \mathbf{e}_1 and \mathbf{e}_2 components. The approximation for the transverse displacement over the whole domain Ω in terms of the set of degrees of freedom $\{w_i\}$ will be expressed as

$$w^h(\{w_i\}) \quad (4.24)$$

whereas the approximation for the rotation field over Ω in the bending and shear

terms will be expressed as

$$\boldsymbol{\psi}_b^h(\{\boldsymbol{\psi}_i\}), \quad \boldsymbol{\psi}_s^h(\{\boldsymbol{\psi}_i\}) \quad (4.25)$$

respectively. Defining the admissible space of degrees of freedoms as

$$\mathcal{U} = \{(\{w_i\}, \{\boldsymbol{\psi}_i\}) \mid w^h(\{w_i\}) = w_g, \boldsymbol{\psi}_b^h(\{\boldsymbol{\psi}_i\}) = \boldsymbol{\psi}_g \quad \text{on } \Gamma_u\} \quad (4.26)$$

and also

$$\mathcal{U}_0 = \{(\{w_i\}, \{\boldsymbol{\psi}_i\}) \mid w^h(\{w_i\}) = 0, \boldsymbol{\psi}_b^h(\{\boldsymbol{\psi}_i\}) = 0 \quad \text{on } \Gamma_u\} \quad (4.27)$$

The discrete variational principal is then to find $(\{w_i\}, \{\boldsymbol{\psi}_i\}) \in \mathcal{U}$ such that

$$\begin{aligned} & \int_{\Omega} (\mathbf{D}_b \boldsymbol{\epsilon}_b(\boldsymbol{\psi}_b^h(\{\boldsymbol{\psi}_i\}))) : \boldsymbol{\epsilon}_b(\boldsymbol{\psi}_b^h(\{\delta\boldsymbol{\psi}_i\})) \, d\Omega + \\ & \int_{\Omega} (\mathbf{D}_s \boldsymbol{\epsilon}_s(w^h(\{w_i\}), \boldsymbol{\psi}_s^h(\{\boldsymbol{\psi}_i\}))) \cdot \boldsymbol{\epsilon}_s(w^h(\{\delta w_i\}), \boldsymbol{\psi}_s^h(\{\delta\boldsymbol{\psi}_i\})) \, d\Omega = \\ & \int_{\Gamma_t} \mathbf{C} \cdot \boldsymbol{\psi}_b^h(\{\delta\boldsymbol{\psi}_i\}) \, ds + \int_{\Gamma_t} \mathbf{T} w^h(\{\delta w_i\}) \, ds \quad \forall (\{\delta w_i\}, \{\delta\boldsymbol{\psi}_i\}) \in \mathcal{U}_0 \end{aligned} \quad (4.28)$$

4.3 Derivation of the Interaction Integral for Plates

In this section, we present the methodology for calculating the mixed-mode moment and shear force intensity factors for through cracks in Mindlin-Reissner plates. We begin by providing a brief summary of the pertinent quantities that arise when dealing with cracks in Mindlin-Reissner plates. The crack tip contour integrals which have previously been developed are reviewed, and we discuss why these integrals are not

well suited for finite element analysis. This discussion motivates the derivation of a domain form of the interaction integral for Mindlin-Reissner plates.

4.3.1 Plate Fracture

Consider the problem of a through crack in a plate as shown in Fig. 4.2, where for convenience we adopt a local polar coordinate system centered at the crack tip. As opposed to the stress intensity factors obtained in classical elasticity, in plate theory the quantities of interest are moment and shear force intensity factors. These are

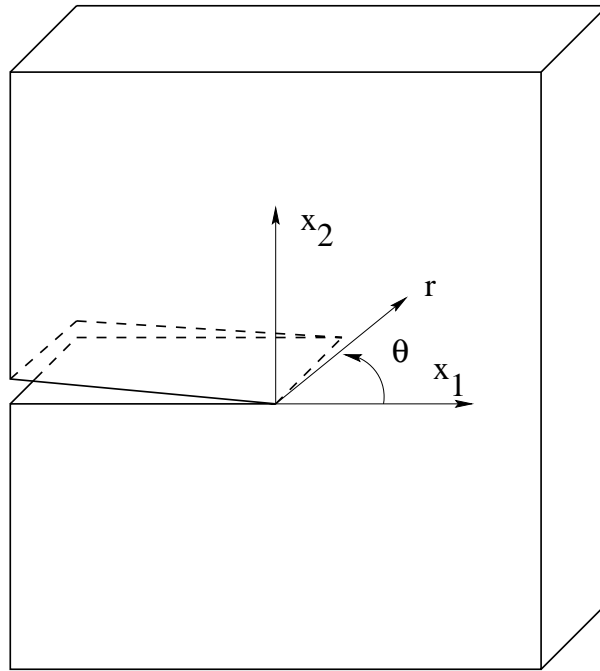


Figure 4.2: Local polar coordinate system for through crack in plate.

defined as

$$K_1 = \lim_{r \rightarrow 0} \sqrt{2r} M_{22}(r, 0), \quad K_2 = \lim_{r \rightarrow 0} \sqrt{2r} M_{12}(r, 0), \quad K_3 = \lim_{r \rightarrow 0} \sqrt{2r} Q_2(r, 0) \quad (4.29)$$

A link to the stress intensity factors of three-dimensional elasticity is made by considering the variation in stress components through the plate thickness. The bending stresses vary linearly through the plate thickness, while the transverse shear stresses vary parabolically. These considerations typically motivate the following relationships

$$k_1(x_3) = \frac{12x_3}{h^3}K_1, \quad k_2(x_3) = \frac{12x_3}{h^3}K_2, \quad k_3(x_3) = \frac{3}{2h} \left[1 - \left(\frac{2x_3}{h} \right)^2 \right] K_3 \quad (4.30)$$

The asymptotic displacement fields in Mindlin-Reissner plate theory can be found in Sosa and Eischen (1986) as a power series in \sqrt{r} . We list here only those terms proportional to \sqrt{r} and $r^{\frac{3}{2}}$:

$$w = \frac{6\sqrt{2r}}{5h\mu}K_3 \sin\left(\frac{\theta}{2}\right) + \frac{6\sqrt{2}r^{\frac{3}{2}}K_1}{Eh^3} \left[\frac{1}{3}(7 + \nu)\cos\left(\frac{3\theta}{2}\right) - (1 - \nu)\cos\left(\frac{\theta}{2}\right) \right] + \quad (4.31a)$$

$$\frac{6\sqrt{2}r^{\frac{3}{2}}K_2}{Eh^3} \left[-\frac{1}{3}(5 + 3\nu)\sin\left(\frac{3\theta}{2}\right) + (1 - \nu)\sin\left(\frac{\theta}{2}\right) \right]$$

$$\psi_1 = \frac{6\sqrt{2r}K_1}{Eh^3} \cos\left(\frac{\theta}{2}\right) [4 - (1 + \nu)(1 + \cos(\theta))] + \frac{6\sqrt{2r}K_2}{Eh^3} \sin\left(\frac{\theta}{2}\right) [4 + (1 + \nu)(1 + \cos(\theta))] + \quad (4.31b)$$

$$\frac{6\sqrt{2}r^{\frac{3}{2}}K_3}{Eh^3} \frac{8}{15} \left[-\sin\left(\frac{\theta}{2}\right) - (1 + 3\nu) \cos\left(\frac{\theta}{2}\right)\sin(\theta) \right]$$

$$\psi_2 = \frac{6\sqrt{2r}K_1}{Eh^3} \left[4 \sin\left(\frac{\theta}{2}\right) - (1 + \nu)(\cos\left(\frac{\theta}{2}\right) \sin(\theta)) \right] + \frac{6\sqrt{2r}K_2}{Eh^3} \left[-2\cos\left(\frac{\theta}{2}\right)(1 - \nu) + (1 + \nu)\sin\left(\frac{\theta}{2}\right) \sin(\theta) \right] + \quad (4.31c)$$

$$\frac{6\sqrt{2}r^{\frac{3}{2}}K_3}{Eh^3} \frac{8}{15} \cos\left(\frac{\theta}{2}\right) [1 + (1 + 3\nu)\cos(\theta)]$$

For the purposes of defining the near-tip enrichment functions in Sec. 4.4 for the plate theory, we consider only the terms proportional to \sqrt{r} for the rotations ψ_1 and ψ_2 .

For the transverse displacement, we consider terms proportional to both \sqrt{r} and $r^{3/2}$.

With these restrictions, the above near-tip fields are contained in the span of the sets

$$w \in \{g_i(r, \theta)\}_{i=1}^5 \quad (4.32a)$$

$$\{\psi_1, \psi_2\} \in \{f_i(r, \theta)\}_{i=1}^4 \quad (4.32b)$$

where

$$\{g_I(r, \theta)\} \equiv \left\{ \sqrt{r} \sin\left(\frac{\theta}{2}\right), r^{\frac{3}{2}} \sin\left(\frac{\theta}{2}\right), r^{\frac{3}{2}} \cos\left(\frac{\theta}{2}\right), r^{\frac{3}{2}} \sin\left(\frac{3\theta}{2}\right), r^{\frac{3}{2}} \cos\left(\frac{3\theta}{2}\right) \right\} \quad (4.33a)$$

$$\{f_I(r, \theta)\} \equiv \left\{ \sqrt{r} \sin\left(\frac{\theta}{2}\right), \sqrt{r} \cos\left(\frac{\theta}{2}\right), \sqrt{r} \sin\left(\frac{\theta}{2}\right) \sin(\theta), \sqrt{r} \cos\left(\frac{\theta}{2}\right) \sin(\theta) \right\} \quad (4.33b)$$

The asymptotic near-tip moment and shear fields obtained from the displacement fields (4.31) are

$$M_{11} = \frac{K_1}{\sqrt{2r}} \cos\left(\frac{\theta}{2}\right) \left(1 - \sin\left(\frac{\theta}{2}\right) \sin\left(\frac{3\theta}{2}\right) \right) - \frac{K_2}{\sqrt{2r}} \sin\left(\frac{\theta}{2}\right) \left(2 + \cos\left(\frac{\theta}{2}\right) \cos\left(\frac{3\theta}{2}\right) \right) \quad (4.34a)$$

$$M_{22} = \frac{K_1}{\sqrt{2r}} \cos\left(\frac{\theta}{2}\right) \left(1 + \sin\left(\frac{\theta}{2}\right) \sin\left(\frac{3\theta}{2}\right) \right) - \frac{K_2}{\sqrt{2r}} \sin\left(\frac{\theta}{2}\right) \cos\left(\frac{\theta}{2}\right) \cos\left(\frac{3\theta}{2}\right) \quad (4.34b)$$

$$M_{12} = \frac{K_1}{\sqrt{2r}} \sin\left(\frac{\theta}{2}\right) \cos\left(\frac{\theta}{2}\right) \cos\left(\frac{3\theta}{2}\right) + \frac{K_2}{\sqrt{2r}} \cos\left(\frac{\theta}{2}\right) \left(1 - \sin\left(\frac{\theta}{2}\right) \sin\left(\frac{3\theta}{2}\right) \right) \quad (4.34c)$$

$$Q_1 = - \frac{K_3}{\sqrt{2r}} \sin\left(\frac{\theta}{2}\right) \quad (4.34d)$$

$$Q_2 = \frac{K_3}{\sqrt{2r}} \cos\left(\frac{\theta}{2}\right) \quad (4.34e)$$

where only the singular terms have been provided.

4.3.2 Available crack-tip contour integrals

Several different domain and path-independent integrals have been developed for the extraction of mixed mode moment and shear force intensity factors in plates, see for example those derived in Sosa and Eischen (1986) or Sosa and Herrmann (1989). We summarize the results of these investigations here in order to motivate the developments which follow. In this section, we use indicial notation where the Greek indices (α, β) range over the values $1 \dots 2$, and a comma denotes a partial derivative with respect to the following argument. We state the restrictions that the following development concerns the case when the crack-faces are traction free and there is no externally applied pressure on the plate.

The development of crack-tip contour integrals begins by considering the appropriate balance, or conservation law. Defining the strain energy in the plate as

$$W = \frac{1}{2} [M_{\alpha\beta}\psi_{\alpha,\beta} + Q_{\beta}(\psi_{\beta} + w_{,\beta})] \quad (4.35)$$

it can be shown that

$$W_{,k} - [M_{\alpha\beta}\psi_{\alpha,k} + Q_{\beta}w_{,k}]_{,\beta} = 0 \quad \text{for } k = 1, 2 \quad (4.36)$$

using the plate equations (4.11), constitutive laws (4.13), (4.14), and strain-displacement relations (4.4), (4.5). The measure numbers J_k are obtained by integrating the above expression over domain A_o enclosed by the contour Γ shown in Fig. 4.3. After applying

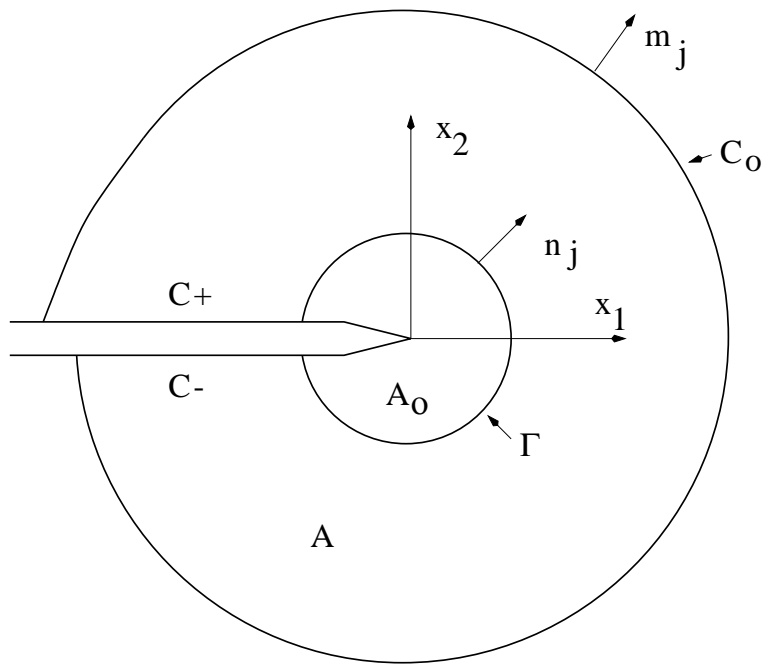


Figure 4.3: Conventions at the crack tip. The domain A_o is enclosed by Γ , while A is enclosed by Γ , C_+ , C_- , and C_o .

the divergence theorem, we arrive at the following:

$$J_k = \oint_{\Gamma} \{W \delta_{k\beta} - [M_{\alpha\beta} \psi_{\alpha,k} + Q_{\beta} w_{,k}]\} n_{\beta} d\Gamma \quad (4.37)$$

The measures J_k vanish when the region enclosed by Γ does not contain a crack. In the present investigation, we are primarily concerned with the J_1 integral. When Γ is an open contour surrounding a crack tip, the J_1 integral is path independent and its magnitude is equivalent to the energy release rate corresponding to a unit crack advance in the x_1 direction.

The relationship between the energy release rate and the moment and shear force intensity factors is determined as follows. The asymptotic fields (4.31) are substituted into the above integral, and a vanishingly small path enclosing the crack tip is considered. In the limit, only the singular terms [$\mathcal{O}(r^{-1})$] contribute to the result

$$J_1 = G = \frac{12\pi}{Eh^3} [K_1^2 + K_2^2] + \frac{\pi}{2k\mu h} K_3^2 \quad (4.38)$$

The calculation of J_1 in conjunction with the above equation is not sufficient to extract $K_1, K_2,$ and K_3 separately. While an analogous relationship can be derived for J_2 , we are still left with only two equations for the three unknowns. To address this issue, Sosa and Herrmann (1989) separated the strain energy into bending and shear contributions as

$$W^b = \frac{1}{2} [M_{\alpha\beta} \psi_{\alpha,\beta}], \quad W^s = \frac{1}{2} [Q_{\beta} (\psi_{\beta} + w_{,\beta})] \quad (4.39)$$

and derived the following integrals from the corresponding conservation laws:

$$J_k^b = \int_{\Gamma} \{W^b \delta_{k\beta} - M_{\alpha\beta} \psi_{\alpha,k}\} n_{\beta} d\Gamma + \int_{A_o} Q_{\beta} \psi_{\beta,k} dA \quad (4.40a)$$

$$J_k^s = \int_{\Gamma} \{W^s \delta_{k\beta} - Q_{\beta} w_{,k}\} n_{\beta} d\Gamma - \int_{A_o} Q_{\beta} \psi_{\beta,k} dA \quad (4.40b)$$

By substituting the near-tip fields into these expressions, the following relationships can be derived:

$$J_1^b = \frac{12\pi}{Et^3} [K_1^2 + K_2^2] \quad (4.41a)$$

$$J_2^b + J_2^s = -\frac{24\pi}{Et^3} K_1 K_2 \quad (4.41b)$$

$$J_1^s = \frac{\pi}{2k\mu t} K_3^2 \quad (4.41c)$$

While the magnitude of K_3 can certainly be determined from (4.41c) above, we cannot discern its sign. Furthermore, the equations (4.41b) and (4.41a) are generally insufficient to separate K_1 and K_2 . A quadratic equation results from solving the system, and the two roots are indistinguishable. While both the sign of K_3 and the separation of K_1 and K_2 may be determined by additionally examining the form of the near-tip fields, this process is fairly cumbersome. An additional concern involves the numerical calculation of the contour integrals (4.40) in a finite element context. When the plate displacements are approximated with $C^0(\Omega)$ continuous shape functions, the moments \mathbf{M} and shears \mathbf{Q} will not be continuous across element boundaries on the contour Γ . This issue is typically addressed by using a ‘smoothing’ technique such as that suggested in Hinton and Campbell (1974). In the sections which follow, we illustrate how the development of the domain form of an interaction integral for plates circumvents all of the aforementioned difficulties.

4.3.3 The Interaction Integral

A particularly convenient method for extracting mixed-mode stress intensity factors is the interaction energy integral approach. Yau, Wang, and Corten (1980) and Shih and Asaro (1988) have employed interaction energy integrals to evaluate mixed-mode stress intensity factors in two-dimensional plane problems, and a review is provided in Appendix A. It is emphasized that in the present investigation, the interaction energy integrals are developed for extracting mixed-mode moment and shear force intensity factors in Mindlin-Reissner plates.

To derive the interaction integral, we begin by considering two states of field quantities: the present state $(\mathbf{M}, \mathbf{Q}, \psi, w)$, and an auxiliary state characterized by $(\mathbf{M}^{aux}, \mathbf{Q}^{aux}, \psi^{aux}, w^{aux})$. The J_1 integral for the sum of the two states is given by

$$J_1^{sum} = \oint_{\Gamma} \{ W^{sum} \delta_{1\beta} - [(M_{\alpha\beta} + M_{\alpha\beta}^{aux})(\psi_{\alpha,1} + \psi_{\alpha,1}^{aux}) + (Q_{\beta} + Q_{\beta}^{aux})(w_{,1} + w_{,1}^{aux})] \} n_{\beta} d\Gamma \quad (4.42)$$

where

$$W^{sum} = \frac{1}{2} [(\mathbf{M} + \mathbf{M}^{aux}) : (\boldsymbol{\epsilon}_b + \boldsymbol{\epsilon}_b^{aux}) + (\mathbf{Q} + \mathbf{Q}^{aux}) \cdot (\boldsymbol{\epsilon}_s + \boldsymbol{\epsilon}_s^{aux})] \quad (4.43)$$

Expanding and rearranging terms gives

$$J_1^{sum} = J_1 + J_1^{aux} + I \quad (4.44)$$

where I is the interaction integral given by

$$I = \oint_{\Gamma} \{W^{int} \delta_{1\beta} - [M_{\alpha\beta} \psi_{\alpha,1}^{aux} + M_{\alpha\beta}^{aux} \psi_{\alpha,1} + Q_{\beta} w_{,1}^{aux} + Q_{\beta}^{aux} w_{,1}]\} n_{\beta} d\Gamma \quad (4.45)$$

and W^{int} is the interaction strain energy

$$W^{int} = \mathbf{M} : \boldsymbol{\epsilon}_b^{aux} + \mathbf{Q} \cdot \boldsymbol{\epsilon}_s^{aux} = \mathbf{M}^{aux} : \boldsymbol{\epsilon}_b + \mathbf{Q}^{aux} \cdot \boldsymbol{\epsilon}_s \quad (4.46)$$

In a similar manner, the energy release rate corresponding to the sum of the present state and the auxiliary state is given by

$$G^{sum} = \frac{12\pi}{Eh^3} [(K_1 + K_1^{aux})^2 + (K_2 + K_2^{aux})^2] + \frac{6\pi}{10\mu h} (K_3 + K_3^{aux})^2 \quad (4.47)$$

Upon rearranging terms we obtain

$$G^{sum} = J_1 + J_1^{aux} + \frac{24\pi}{Eh^3} [K_1 K_1^{aux} + K_2 K_2^{aux}] + \frac{12\pi}{10\mu h} K_3 K_3^{aux} \quad (4.48)$$

By equating J^{sum} in (4.44) with G^{sum} , we arrive at the following relationship:

$$I = \frac{24\pi}{Eh^3} [K_1 K_1^{aux} + K_2 K_2^{aux}] + \frac{12\pi}{10\mu h} K_3 K_3^{aux} \quad (4.49)$$

The auxiliary state is set to the leading order terms in the expressions for the exact near-tip fields (4.31) and (4.34). For the near-tip displacements, only those terms proportional to \sqrt{r} are taken. The process of evaluating the mixed-mode intensity factors involves making a judicious choice of the auxiliary moment and shear force intensity factors, and then evaluating the interaction energy integral (4.45). For

example, to extract K_1 , we set $K_1^{aux} = 1$, $K_2^{aux} = 0$, $K_3^{aux} = 0$, from which it follows from the above that

$$K_1 = \frac{Eh^3}{24\pi} I \quad (4.50)$$

The moment and shear force intensity factors K_2 and K_3 are extracted in a similar fashion. In order to numerically evaluate the interaction integral, it is advantageous to recast the contour integrals in their equivalent domain forms which are developed in the following section.

4.3.4 Domain Form of the Interaction Integral

In this section, we illustrate the use of a weight function q to recast the line integrals developed in the previous section into their equivalent domain form. The domain forms are particularly well suited for use with finite elements, as the same quadrature points used for the construction of the bilinear form can be used to calculate the domain integral. Additional quadrature points or the use of a smoothing procedure are not required.

We begin with the contour integral presented in the last section (4.45). Consider the simply connected curve $C = C_o + C_+ + C_- + \Gamma$ as shown in Fig. 4.3. Following Moran and Shih (1987), we now introduce a weight function q which is sufficiently smooth in the area A enclosed by C , and is defined on the surfaces as:

$$q = \begin{cases} 1 & \text{on } \Gamma \\ 0 & \text{on } C_o \end{cases} \quad (4.51)$$

We then use this function to rewrite (4.45) as

$$I = \oint_C \{ -W^{int} \delta_{1\beta} + [M_{\alpha\beta} \psi_{\alpha,1}^{aux} + M_{\alpha\beta}^{aux} \psi_{\alpha,1} + Q_{\beta} w_{,1}^{aux} + Q_{\beta}^{aux} w_{,1}] \} m_{\beta} q \, dC - \int_{C_+ + C_-} [M_{\alpha 2} \psi_{\alpha,1}^{aux} + M_{\alpha 2}^{aux} \psi_{\alpha,1} + Q_2 w_{,1}^{aux} + Q_2^{aux} w_{,1}] m_2 q \, dC \quad (4.52)$$

where we have used $m_i = n_i$ on C_o , $m_i = -n_i$ on Γ , and $m_1 = 0, m_2 = \pm 1$ on the crack faces. The last integral above vanishes for traction free crack faces. Applying the divergence theorem to the integral over A , we obtain

$$I = \int_A \{ [M_{\alpha\beta} \psi_{\alpha,1}^{aux} + M_{\alpha\beta}^{aux} \psi_{\alpha,1} + Q_{\beta} w_{,1}^{aux} + Q_{\beta}^{aux} w_{,1}] - W^{int} \delta_{1\beta} \} q_{,\beta} \, dA + \int_A \{ [M_{\alpha\beta} \psi_{\alpha,1}^{aux} + M_{\alpha\beta}^{aux} \psi_{\alpha,1} + Q_{\beta} w_{,1}^{aux} + Q_{\beta}^{aux} w_{,1}] - W^{int} \delta_{1\beta} \}_{,\beta} q \, dA \quad (4.53)$$

The integrand in the second integral above needs to be examined in more detail. If the auxiliary fields satisfy the strain-displacement equations (4.4), (4.5), the constitutive equations (4.13), (4.14), and the equilibrium equations (4.11), then this integrand will vanish. When the auxiliary fields are chosen to be the leading order terms in r , however, either the equilibrium equations or the strain-displacement relationships will not be satisfied exactly. For example, in the case when the auxiliary fields correspond to a pure K_1 state, we have from (4.34) that

$$\mathbf{Q}^{aux} = 0, \quad \boldsymbol{\epsilon}_s^{aux} = 0 \quad (4.54)$$

and yet from (4.31) the section rotations are non-zero, and so the strain displacement relationship (4.5) is not satisfied. A similar situation arises when the auxiliary fields

correspond to a pure K_2 state, and when the case is pure K_3 we have

$$\mathbf{M}^{aux} = 0, \quad \nabla \cdot \mathbf{M}^{aux} = 0 \tag{4.55}$$

and yet the auxiliary shears are non-zero and so the equilibrium equations are not satisfied.

After a good deal of algebraic manipulations, the appropriate cancellations can be made to reduce (4.53) to the following domain form of the interaction integral:

$$\begin{aligned} I = \int_A \{ [M_{\alpha\beta} \psi_{\alpha,1}^{aux} + M_{\alpha\beta}^{aux} \psi_{\alpha,1} + Q_{\beta} w_{,1}^{aux} + Q_{\beta}^{aux} w_{,1}] - W^{int} \delta_{1\beta} \} q_{,\beta} \, dA + \\ \int_A \{ (M_{\alpha\beta,\beta}^{aux} - Q_{\alpha}^{aux}) \psi_{\alpha,1} + Q_{\alpha} (w_{,\alpha 1}^{aux} + \psi_{\alpha,1}^{aux} - \epsilon_{s \alpha,1}^{aux}) \} q \, dA \end{aligned} \tag{4.56}$$

We remark that it is necessary to include the terms in the second integral to preserve the domain independence of the measure number I .

The above integral can be reduced depending on whether the quantity of interest is K_1 , K_2 , or K_3 , as certain terms in the auxiliary fields vanish for each case. For example, for K_1 and K_2 the integral takes the form

$$I = \int_A \{ [M_{\alpha\beta} \psi_{\alpha,1}^{aux} + M_{\alpha\beta}^{aux} \psi_{\alpha,1}] - W^{int} \delta_{1\beta} \} q_{,\beta} \, dA + \int_A (Q_{\alpha} \psi_{\alpha,1}^{aux}) q \, dA \tag{4.57}$$

whereas for K_3 the integral reads

$$I = \int_A \{ [Q_{\beta} w_{,1}^{aux} + Q_{\beta}^{aux} w_{,1}] - W^{int} \delta_{1\beta} \} q_{,\beta} \, dA - \int_A (Q_{\alpha}^{aux} \psi_{\alpha,1}) q \, dA \tag{4.58}$$

It is noted that the above forms are similar to the bending and shear integrals (4.40) presented earlier. In fact, the above forms can also be derived by considering (4.40)

for the sum of two states, and then performing the same manipulations presented in this section.

Finally, if the auxiliary state variables are set to the present variables in the interaction integral, we recover the domain form of the J_1 integral for plates. This is given by

$$J_1 = \int_A \{ [M_{\alpha\beta}\psi_{\alpha,1} + Q_{\beta}w_{,1}] - W\delta_{1\beta} \} q_{1,\beta} dA - \int_{C_+ + C_-} [M_{\alpha 2}\psi_{\alpha,1} + Q_2 w_{,1}] m_2 q_1 dC \quad (4.59)$$

It is useful to calculate the above integral as a check on the value of the energy release rate G obtained from the interaction integral. For example, once K_1 , K_2 , and K_3 have been determined using three separate calculations of the interaction integral and (4.49), the energy release rate can be obtained from (4.38) and compared to J_1 .

4.4 Enriched MITC Approximation

We construct an enriched MITC approximation in much the same way as in Chapter 3. The main difference is the enrichment of the transverse displacement and rotations with different sets of near-tip fields. The enriched approximation takes the form

$$w^h(\mathbf{x}) = \sum_{i \in I} \phi_i w_i + \sum_{j \in J} \phi_j H(\mathbf{x}) b_j^w + \sum_{k \in K} \phi_k \left(\sum_{l=1}^4 c_{kl}^w G_l(r, \theta) \right) \quad (4.60a)$$

$$\psi^h(\mathbf{x}) = \sum_{i \in I} \tilde{\phi}_i \psi_i + \sum_{j \in J} \tilde{\phi}_j H(\mathbf{x}) \mathbf{b}_j^\psi + \sum_{k \in K} \tilde{\phi}_k \left(\sum_{l=1}^4 \mathbf{c}_{kl}^\psi F_l(r, \theta) \right) \quad (4.60b)$$

where ϕ_i are the standard bilinear shape functions. The sets of nodes J and K are determined from the interaction of the crack and mesh geometries as described in

Section 3.3.

The sets of near-tip functions G_l and F_l are derived from (4.33) in the following fashion. We take G_l to be only those functions in g_l which are proportional to $r^{3/2}$. The set F_l is taken to be equivalent to f_l . In addition to having four additional degrees of freedom for each displacement component, this choice for G_l and F_l satisfies the following relation

$$\nabla G_l(r, \theta) \in \text{span } F_l(r, \theta) \quad (4.61)$$

such that a linear combination of the near-tip enrichment functions can satisfy (4.20). Unfortunately, this relationship does not ensure that the enriched formulation will be completely free of shear locking. The above choices for the functions F_l and G_l were found to give the best overall results in terms of the performance with varying plate thickness and the accuracy of moment and shear force intensity factors. The studies presented in the next section provide further insight.

4.5 Numerical examples

In this section, we present some examples using the enriched MITC4 plate formulation. We first examine the accuracy of the method as a function of plate thickness for a benchmark problem, and then present a more general example. Throughout this section, the material properties are assumed to be isotropic with Young's modulus $E = 200$ GPa and Poisson's ratio $\nu = 0.3$.

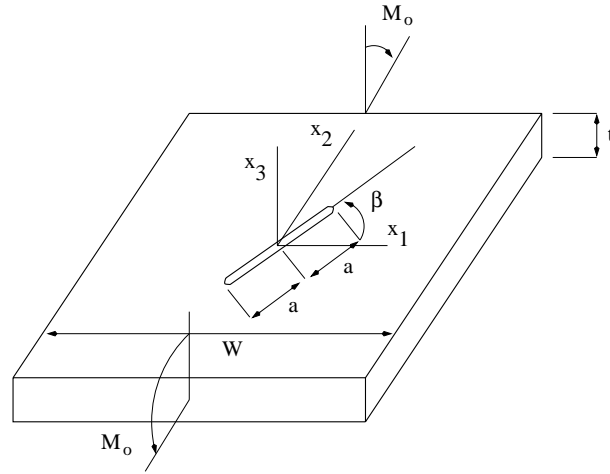


Figure 4.4: Loading configuration for bending of cracked plate.

4.5.1 Benchmark problem

As a benchmark problem we consider a through crack in an infinite plate subjected to a far-field moment M_o . The crack is oriented at an angle β with respect to the x_1 axis as shown in Fig. 4.4. Very accurate calculations were carried out by Joseph and Erdogan (1991) for various plate thicknesses for $\beta = 0^\circ$. In this configuration, the loading is purely mode I , and the domain form of the J-integral for plates (4.59) is used in conjunction with (4.38) to determine the moment intensity factor K_I . We also take advantage of the symmetry about the x_2 axis (when $\beta = 0$) and model only one-half of the plate with finite elements. To approximate the infinite plate, the plate width W is taken to be 20 times the half crack length a . The crack length is taken to be $2a = 1.0$ for the results presented in this study .

Fig. 4.5 shows the normalized K_I for four discretizations, two with enrichment and two without. The lower curve corresponds to a standard MITC4 approximation, and the values for K_I are within 5% of the exact for the entire range of plate thicknesses.

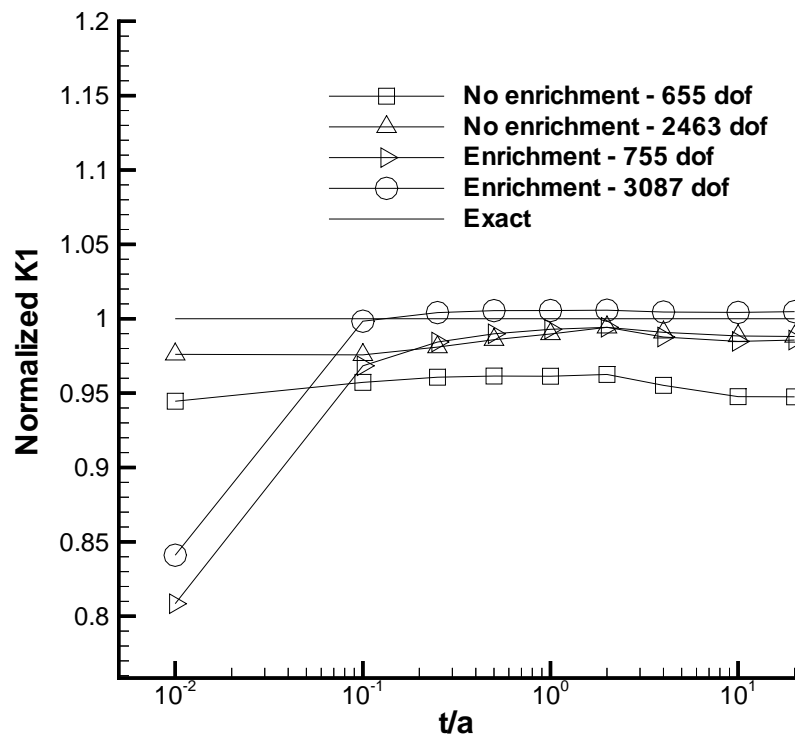


Figure 4.5: Normalized moment intensity factors for varying plate thickness.

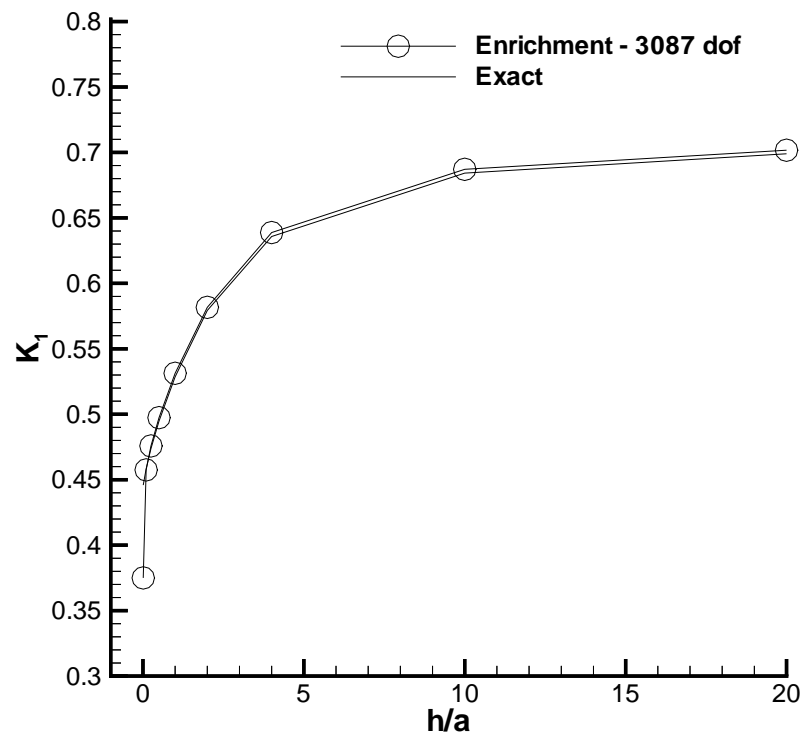


Figure 4.6: Normalized moment intensity factors for varying plate thickness.

These values are improved when the mesh is refined for a total of 2463 degrees of freedom as shown. We observe that the solution obtained with the enriched approximation and only 755 degrees of freedom is as accurate as the standard approximation with 2463 degrees of freedom. The last curve for the enriched case with 3087 degrees of freedom exhibits less than 1% error. An exception concerns both enriched solutions when the normalized thickness $t/a = 0.01$, where a significant decrease in accuracy is observed. This deviation may be attributed to the onset of shear locking for the enriched approximation. We note that this occurs only for very thin plates ($h/W = 1/2000$), and that the calculated moment intensity factor K_1 for $h/a = 0.1$ is within 3% of the limiting value of 0.4439. This is illustrated in Fig. 4.6 where the moment intensity factor is not normalized.

Additional moment intensity factors are calculated for a finite plate as a function of crack length for various plate thicknesses. The geometry of the plate is taken to be the same as in the previous example, and the results are compared to those given in Boduroglu and Erdogan (1983). In this study, the mesh does not model the crack discontinuity; the jump in the rotations and transverse displacement is created entirely with enrichment. Table 4.1 gives the results for four different width to thickness ratios for the case when the plate is modeled with 1424 MITC4 elements. These results show excellent correlation for the cases when $t = w/4$ and $t = w/8$, in which the maximum error is 1.2%. For the remaining cases the maximum difference between the numerical solutions and those given in Boduroglu and Erdogan (1983) is 9.4%. We remark that the results given in Boduroglu and Erdogan (1983) are not as reliable as those found in Joseph and Erdogan (1991). In the latter, the moment intensity factors are shown to be significantly greater than the classical results (Sih, 1977) as the thickness $t \rightarrow 0$. The results shown in Table 4.1 are consistent with

$t = w/4$		$t = w/8$		$t = w/12$		$t = w/16$	
$\frac{a}{w}$	$\frac{K_I}{K_I^{exact}}$	$\frac{a}{w}$	$\frac{K_I}{K_I^{exact}}$	$\frac{a}{w}$	$\frac{K_I}{K_I^{exact}}$	$\frac{a}{w}$	$\frac{K_I}{K_I^{exact}}$
0.025	0.988	0.025	0.989	0.0333	1.067	0.0250	1.077
0.05	0.992	0.050	0.993	0.0500	1.052	0.0375	1.090
0.10	0.997	0.075	0.995	0.0667	1.069	0.0500	1.094
0.20	1.000	0.100	0.996	0.0833	1.070	0.0625	1.092
0.25	0.999	0.125	0.997	0.1667	1.054	0.1250	1.072
0.333	1.013	0.250	0.998	0.3333	1.057	0.2500	1.062

Table 4.1: Normalized K_I values for finite plate.

these findings.

4.5.2 Angled center crack

We now present results for the moment and shear force intensity factors as a function of the angle β for the geometry of Fig. 4.4. These results serve to illustrate the versatility of the present formulation, as well as the validity of the interaction integral derived in Section 4.3.4.

We consider the case of a relatively thick plate, by taking $t/a = 2$. The exact solution for the infinite plate is given in Sih (1977) as

$$K_1 = \Phi(1)M_o\sqrt{a} \cos^2\beta \quad (4.62a)$$

$$K_2 = \Psi(1)M_o\sqrt{a} \cos\beta \sin\beta \quad (4.62b)$$

$$K_3 = -\frac{\sqrt{10}}{(1+\nu)t}\Omega(1)M_o\sqrt{a} \cos\beta \sin\beta \quad (4.62c)$$

where the functions $\Phi(1)$, $\Psi(1)$, and $\Omega(1)$ are computed numerically from integral equations. When $t/a = 2$, these are approximately 0.82, 0.68 and 0.06, respectively.

We remark that Joseph and Erdogan (1991) have questioned the validity of the above relationships for thinner plates.

We present results as a function of β for two situations. In the first case, a portion of the mesh is rotated such that the element edges align with the geometry of the crack. A typical mesh of 1920 MITC4 elements is shown in Fig. 4.7. In the second case, the same number of elements is used but the mesh is not rotated and the crack cuts across element boundaries. In all configurations, the plate displacements are discretized with the enriched MITC4 approximation (4.60).

Fig. 4.8 shows the results when the crack aligns with the mesh. The numerical results show good correlation with the exact values for the full range of β . The results for a fixed mesh are shown in Fig. 4.9. While the agreement between the numerical and the exact results for K_1 and K_2 is acceptable, there is substantial deviation in K_3 . From (4.34), we observe that there is a strong relationship between the shear force intensity factor and the shear fields \mathbf{Q} . For pure K_3 loading, only the shears Q_1 and Q_2 are singular. As the approximation for the shear is also modified by the MITC formulation to avoid locking, we can conclude from these studies that a crack cutting across element boundaries adversely affects this approximation. An improvement in the results is achievable with finer discretization, and Fig. 4.10 shows the results using a mesh of 4080 MITC4 elements. Despite doubling the number of elements, some oscillations are still observable for K_3 .

4.6 Closing Remarks

In this chapter, an enriched formulation for plate fracture in the Mindlin-Reissner framework has been presented. The form of the enriched approximation is similar to

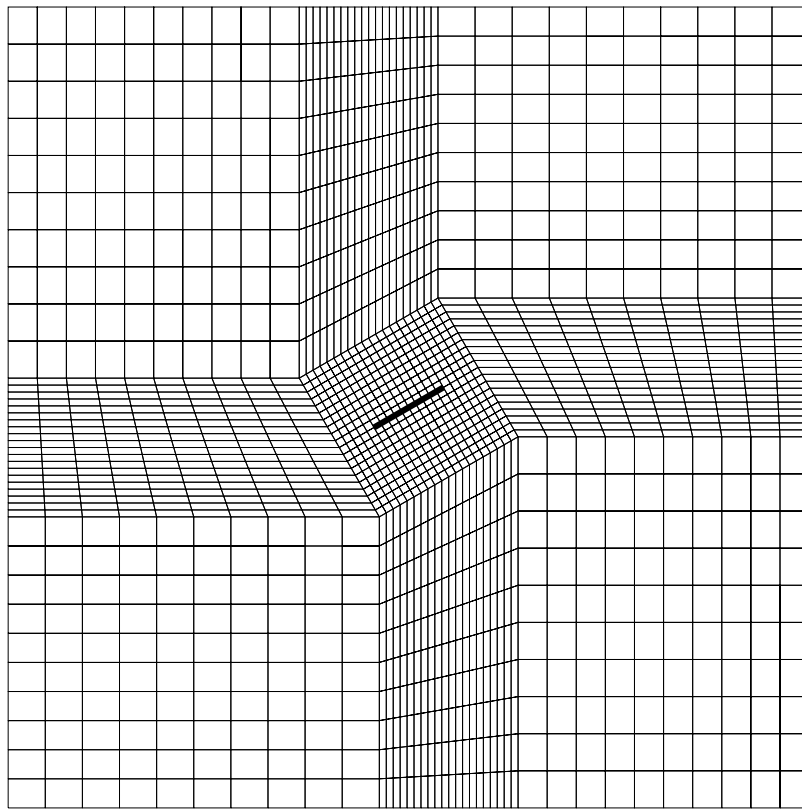


Figure 4.7: Mesh with typical rotated center section. The crack geometry is shown in bold.

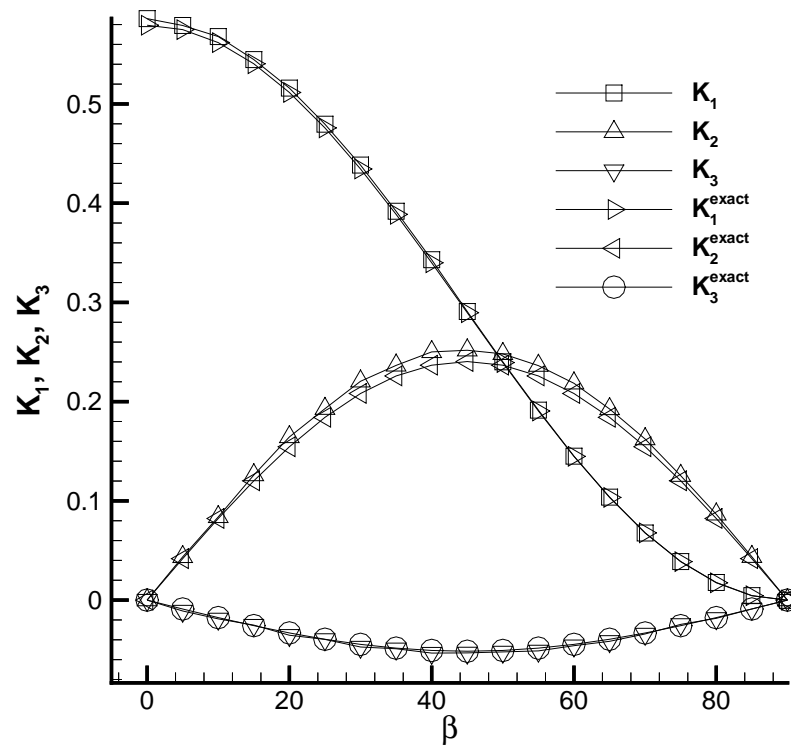


Figure 4.8: Normalized moment and shear force intensity factors for center crack at angle β . The crack is aligned with the mesh.

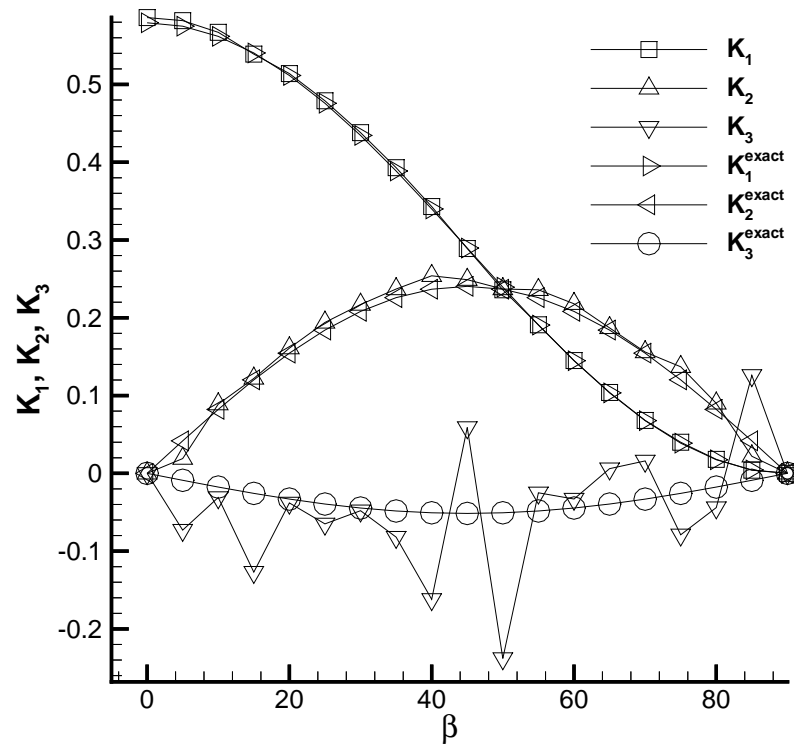


Figure 4.9: Normalized moment and shear force intensity factors for center crack at angle β . The crack is not aligned with the mesh.

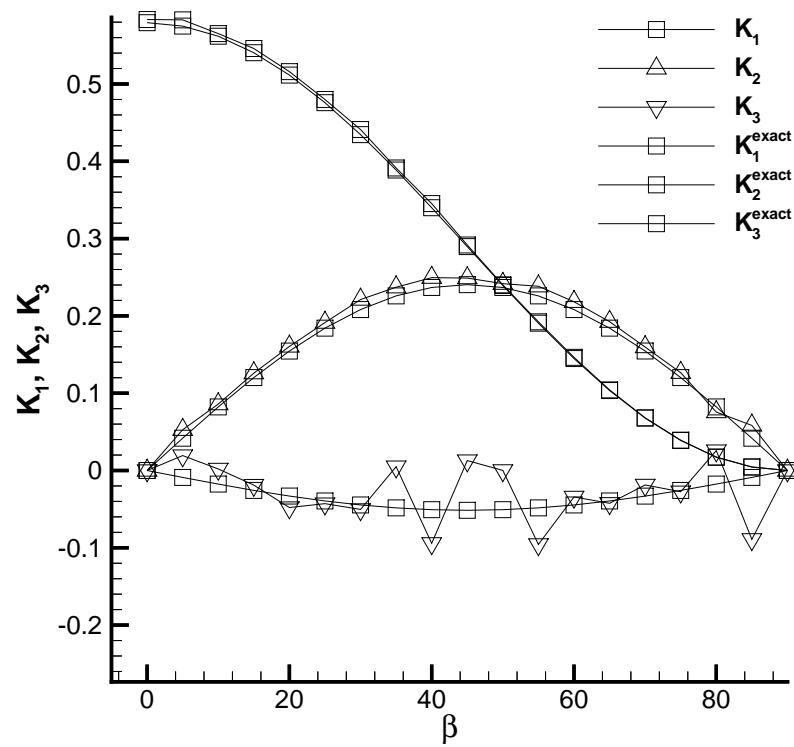


Figure 4.10: Normalized moment and shear force intensity factors for center crack at angle β . The crack is not aligned with the mesh of 4080 MITC4 elements.

that derived in Chapter 3, with different sets of near-tip functions for the rotations and transverse displacement. In order to extract the mixed-mode intensity factors, appropriate domain forms of the interaction integral were derived. A key component to the success of the domain integrals is the incorporation of terms which arise from the failure of the auxiliary fields to satisfy the equilibrium and strain-displacement equations. Several benchmark problems illustrated good performance for the formulation, and only a small amount of shear locking was evident. Some adverse effects of the enrichment were also noticed in the calculation of the shear force intensity factor, especially when the crack cut across element boundaries.

The construction of an enriched approximation for Mindlin-Reissner plates which completely avoids shear locking may be difficult. The selection of approximating spaces which do not exhibit shear locking are usually formulated in terms of the element shape functions. A difficulty with the enriched basis functions is that they are constructed using both the element and crack geometries, as opposed to just a map with a parent element. It is precisely this construction which gives the enriched formulation the flexibility to model cracks which are not oriented with the mesh. It may be possible to construct an enrichment scheme which avoids shear locking when the element and crack geometries are aligned, and this is an area for future work.